J. Phys. B: At. Mol. Opt. Phys. **33** (2000) 265–283. Printed in the UK PII: S0953-4075(00)07935-9

Photodouble ionization of helium at an excess energy of 40 eV

S Cvejanović†, J P Wightman†, T J Reddish†, F Maulbetsch†,
M A MacDonald‡, A S Kheifets§ and I Bray‖

† Physics Department, The University of Newcastle, Newcastle upon Tyne NE1 7RU, UK
‡ CLRC, Daresbury Laboratory, Daresbury, Warrington WA4 4AD, UK
§ Research School of Physical Sciences and Engineering, Australian National University, Canberra, ACT 0200, Australia
‖ Electronic Structure of Materials Centre, Flinders University of South Australia, GPO Box 2100, Adelaide, SA 5001, Australia

Received 20 September 1999

Abstract. Angular correlation in the two-electron continuum of the He double photoionization has been studied, both experimentally and theoretically, for equal and unequal energy sharing conditions at the photon energy of 40 eV above the threshold. The triple differential cross sections have been measured in the plane perpendicular to the photon direction using the multi-coincidence detection technique of Reddish *et al* at the Daresbury Synchrotron Radiation Source. Recent modifications to the bending-magnet beam line allowed an effective cancellation of the circular polarization at the target, leaving a relatively high degree of linear polarization (Stokes parameters: $S_3 = S_2 \cong 0$, $S_1 = 0.8$). The measured cross sections are compared with the calculations using the 3C method of Maulbetsch and Briggs and the convergent close coupling method of Kheifets and Bray. Good agreement between theory and experiment has been found in most cases, except for the unequal energy sharing when one of the escaping electrons is detected in a direction close to the polarization axis.

1. Introduction

The study of the angular distribution of escaping photoelectrons in the photodouble ionization (PDI) of helium is of paramount importance for understanding the role of electron correlations in this most fundamental Coulomb system of three unbound particles. Research in this relatively new field is presently enjoying a surge in activity due to the availability of new experimental techniques of increasing sophistication, yielding a growing body of data with which the developing theories can be tested. The incident photons are provided exclusively by synchrotron radiation sources, due to the requirement that a single photon possesses an energy that is higher than the double ionization threshold (79 eV). Since the pioneering work of Schwarzkopf *et al* (1993), the helium triple differential cross section (TDCS) has been measured by a variety of experimental schemes for coincident detection of electrons that could be broadly sub-divided into single- and multi-detection techniques. The most successful single-detection systems have been described by Krässig *et al* (1993) and Dawber *et al* (1995). An example of a multi-detector is the system of two time-of-flight electron energy analysers (Viefhaus *et al* 1996a), offering a 'simultaneous' detection of coincidences for a chosen orientation of detected electrons but an arbitrary sharing of the available energy. Alternatively, one can adopt—as in this work—a scheme consisting of two energy analysers, of which at least one simultaneously covers a large range of emission angles while still being able

0953-4075/00/020265+19$30.00

to distinguish between them (Mazeau *et al* 1997, Reddish *et al* 1997a). These multi-detector arrangements provide a valuable increase in sensitivity over the single-detection systems, which makes measurements of a very small coincident yield feasible.

Another technique, which combines the features of the two multi-detection schemes described above, is cold-target recoil-ion momentum spectroscopy, COLTRIMS (see Dörner *et al* 1998). It is based on detecting one of the two ejected electrons in coincidence with the recoiling ion from a pre-cooled supersonic expansion gas source. Energy and momentum conservation laws enable the extraction of the kinematic properties of the undetected electron. A combination of electric and magnetic fields and field-free drift regions was used to project emitted electrons and recoiled ions onto the separate position-sensitive detectors. In this way the authors were able to observe simultaneously the coincident events between all the ions and the electrons of arbitrary energy ejected over a large solid angle, up to the full 4π sr (Bräuning *et al* 1998, Dörner *et al* 1998). This experimental scheme yields three-dimensional TDCSs that could be internally calibrated and placed on an absolute scale. The unique potential of this method has yet to be matched with the energy/angular resolution and statistical accuracy more routinely available in the electron-pair detection methods.

It was clear from the outset that the simultaneous ejection of two electrons by a single photon involves mutual interaction between the atomic electrons. The classical study by Wannier (1953) of the helium break-up process close to threshold and the subsequent confirmations of the predicted threshold laws (Brion and Thomas 1968, Cvejanović and Read 1974) firmly established the important role of the Coulomb interaction in the exit channel. Wannier-type treatments and their semiclassical extensions (Vinkalns and Gailitis 1967, Peterkop 1971, Rau 1971) focused on the electron's dynamics in the outer region of the interaction space. They assume a highly correlated (yet unstable) motion of the escaping electrons along the 'Wannier ridge' ($r_1 \sim r_2$) and work best at small energies, although successful attempts at extending the theory to more general conditions have been made (Kazansky and Ostrovsky 1994, 1995a, b, Feagin 1995, 1996, Dörner *et al* 1998).

Highly successful quantum mechanical treatments have been developed too, combining the concept of detailed representation of the electron interactions in the final state with the inclusion of the correlations in the initial state. The pioneering work was done by Maulbetsch and Briggs (1993, 1994) who used a product wavefunction (3C) to describe the final continuum state. In this approach both the initial and final wavefunctions are known analytically. This knowledge can be of immense value and is used extensively to gain insight into the mechanisms underlying the ionization process and the origins of features in the cross section. Both length and velocity forms of the cross sections are calculated to give an indication of the quality of the results. Of course, gauge sensitivity is a direct result of the approximate nature of the wavefunctions used, a point that has been investigated in detail by Lucey *et al* (1998).

The other theories are fundamentally different in that they use some form of basis set expansion that should, in principle, result in accurate results if the number of states included in the calculation can be made large enough. The computationally more demanding method of Pont and Shakeshaft (1995a, b), who used the screened Coulomb functions (2SC) to describe the final state, gave well converged and reliable absolute cross sections. The convergent close coupling (CCC) formalism (Kheifets and Bray 1998a) is another method based on an expansion and achieves an essentially gauge-invariant description of the PDI. This method is also capable of producing accurate total cross sections (Kheifets and Bray 1998b). All theories calculate the total cross section by integrating the TDCS (for a particular state of light polarization) over the appropriate momentum space. The agreement between the calculated TDCSs and the relative measurements for equal-energy sharing or close to threshold are generally very good (see Maulbetsch *et al* 1995, Kheifets and Bray 1998a). However, some experimental data for

unequal sharing (Lablanquie *et al* 1995, Bräuning *et al* 1998, Mergel *et al* 1998) could not be satisfactorily reproduced by any theory, which helped to identify the domains of electron kinematics for which not only the agreement between experiment and theory was poor but also large differences between the theories existed (see Pont *et al* 1996, Kheifets and Bray 1998c). Our present work is a systematic study of helium PDI TDCS under conditions which enable a stringent test of existing theories.

For a unified view of different aspects of the experimental and theoretical results one needs a decomposition of the general TDCS into a limited number of suitably selected components. A general expression separating the contributions of different polarization states of incident radiation for any photoabsorption process is (see Schaphorst *et al* 1995)

$$\sigma = \frac{1}{2}(\sigma_x + \sigma_y) + \frac{S_1}{2}(\sigma_x - \sigma_y) + \frac{S_3}{2}(\sigma_r - \sigma_l) \tag{1}$$

where S_1 and S_3 are the Stokes parameters determining the relative contribution of linearly and circularly polarized components, with the x-axis of the Cartesian coordinate system aligned with the main axis of the polarization ellipse (i.e. $S_2 = 0$). In the following we will take σ to represent the TDCS, with lower indices denoting its value for the specific component of the light polarization—(x, y) for the two orthogonal orientations of the linear polarization vector and (r, l) for the two opposite helicity components (right, left) of the circularly polarized light. Note the first term, which is polarization insensitive and, as such, can also be defined in terms of the circular polarization components:

$$^{pi}\sigma = \tfrac{1}{2}(\sigma_x + \sigma_y) = \tfrac{1}{2}(\sigma_r + \sigma_l). \tag{2}$$

The second and third parentheses in (1) contain the so-called linear and circular dichroisms (LD, CD), quantities which represent the differential sensitivity of the TDCS to those two types of light polarization.

A general parametrization of the TDCS for various states of light polarization and symmetries of the atomic target states has been pursued by Klar and collaborators (Berakdar and Klar 1992 and references therein) and Huetz and collaborators (Huetz *et al* 1991, Malegat *et al* 1997a). The work of the latter group, in particular, has provided an indispensable tool for the discussion of the features of the TDCS through physically appealing separation of the effects of electron dynamics from the kinematical and symmetry effects which are particular to the geometry of the experiment and the ionic state symmetry. To see what physical information is contained in the various terms of expression (1) for our experimental geometry (electron detectors in the plane perpendicular to the photon direction, with their angles θ_i measured with respect to the linear polarization direction), one can follow Huetz *et al* (1994) and Malegat *et al* (1997a) to extract the appropriate forms of the partial cross sections. For the overall $^1\mathrm{P}^o$ state symmetry (which applies to He) and disregarding the spins of the detected electrons, the TDCS for the light which is linearly polarized along the x-axis becomes

$$\sigma_x = |(\cos\theta_1 + \cos\theta_2)a_\mathrm{g} + (\cos\theta_1 - \cos\theta_2)a_\mathrm{u}|^2. \tag{3}$$

This contains two complex amplitudes, one symmetric (a_g) and the other one antisymmetric (a_u) with respect to the exchange of electron energies. These amplitudes contain all the information about the dynamics of the process and are, in general, functions of the sum of electron energies E, the way they share it, $R = E_2/E_1$, and their mutual angles θ_{12}. The parametrization (3) is particularly suitable for the symmetric sharing TDCS, as for $R = 1$ the ungerade amplitude (a_u) is zero and $|a_\mathrm{g}|^2$ (the 'correlation function') acquires a form that has been found to be very nearly Gaussian with its peak at $\theta_{12} = \pi$ (see Malegat *et al* 1997b). In the case of unequal energies the contributions of the ungerade term cannot be separated from the gerade except for $\theta_{12} \cong \pi$, as for this mutual angle the kinematical factors in (3) strongly favour the ungerade term.

The counterpart of equation (3) for the linear polarization along the y-axis, σ_y, is obtained by replacing cosine with sine in the above expression. The substitution of these two expressions into the first part of equation (2) yields a relatively simple form for the polarization-insensitive term

$$^{pi}\sigma = (1 + \cos\theta_{12}) \cdot |a_{\mathrm{g}}|^2 + (1 - \cos\theta_{12}) \cdot |a_{\mathrm{u}}|^2 \tag{4}$$

which contains an incoherent sum over the two symmetry components and only the mutual angles in the kinematical factors.

The LD term follows in a straightforward manner but is not shown here explicitly due to its complex appearance. This is due to the dependence of its kinematical factors on the individual angles θ_1, θ_2 and because it additionally depends on $|a_{\mathrm{g}}(\theta_{12})| \cdot |a_{\mathrm{u}}(\theta_{12})| \cdot \cos(\phi)$, ϕ being the phase difference between the amplitudes. To complete the parametrization of equation (1) a parametric form of the CD term is required. It was established earlier that the CD term disappears if the observational plane contains the photon beam direction, $\boldsymbol{k}_\gamma$ (see Berakdar *et al* 1993). Our experimental geometry, where the electrons are detected in the plane perpendicular to $\boldsymbol{k}_\gamma$, is, however, kinematically favoured for its observation. From the expressions for the TDCS for pure circular polarization (Malegat *et al* 1997a) one obtains

$$CD = -4\sin(\theta_{12}) \cdot |a_{\mathrm{g}}(\theta_{12})| \cdot |a_{\mathrm{u}}(\theta_{12})| \cdot \sin(\phi) \tag{5}$$

which contains the same cross section normalization as in (3) and (4). For $E_1 = E_2$ the CD term is identically zero, as for this condition the ungerade amplitude is zero. But when $E_1 \neq E_2$ this is not generally the case, resulting in circular dichroism. The first measurements of the direct CD effect in the PDI of helium have been reported by Viefhaus *et al* (1996b), followed by Mergel *et al* (1998), Soejima *et al* (1999) and Kheifets *et al* (1999), but that interesting topic will not be further discussed here as we are primarily concerned with linearly polarized light in these experiments.

This brief review of the structure of the general cross section expression shows that measurements with either a linearly or a circularly polarized source provide complementary information on the phase relation between the a_{g} and a_{u} amplitudes, requiring a mixed polarization state for a 'complete' experiment. If one could deduce, in a unique way, those amplitudes from measured or calculated TDCSs they would become convenient objects for discussing the effects of electron correlations irrespective of the actual conditions of the experiment, and perhaps open the way for the general parametrization of TDCS for arbitrary dynamical conditions (see a recent review by Schmidt (1998) for further elaboration).

In the remainder of the text we present the first comprehensive set of TDCSs measured at 40 eV above threshold in the perpendicular plane geometry, for equal ($R = 1$) and unequal ($R = 3, 7$) energy sharing and partially polarized radiation given by Stokes parameters $S_2 = S_3 = 0$, $S_1 = 0.8$. All individual TDCSs were subjected to the comparisons with the theoretical predictions of the 3C and CCC theories with which the qualitative agreement is generally good. The remaining differences are discussed in terms of the ratios of the gerade and ungerade amplitudes and their phase difference.

2. Experimental details

The (γ, 2e) experiments were performed at the Daresbury SRS (beam line 3.3) using a coincidence spectrometer based on a toroidal geometry. That apparatus and measurement technique has been described in detail elsewhere (Reddish *et al* 1997a, Wightman *et al* 1998). Briefly, the photon beam is crossed with an effusive gas jet emanating from a hypodermic needle. Photoelectrons emitted in the plane orthogonal to the photon beam direction ($\boldsymbol{k}_\gamma$)

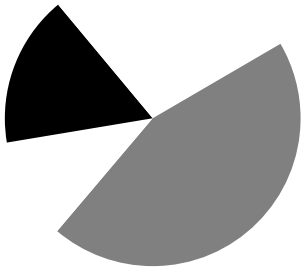

Figure 1. A schematic diagram of the acceptance angle ranges and the mutual configuration of the two toroidal analysers in our 'perpendicular plane' geometry. The (γ, 2e) coincidence signal corresponds to energy-resolved electrons with emission angles within the 60° (black) sector and the 160° (dark grey) sector, having energies designated as E_1 and E_2, respectively. The relative orientation of the two analysers is fixed, but the whole spectrometer can rotate around the photon beam direction, so sampling different aspects of the angular distributions for the linearly polarized light source.

are energy analysed by two toroidal analysers with the acceptance angles and configuration indicated in figure 1. The focusing properties of these electrostatic analysers allow the electron emission angles (measured relative to the light polarization axis) to be mapped onto 2D resistive anode encoders. The images on these detectors are circular arcs in shape, with positions around the perimeter corresponding to the electron emission angles. True coincidences between the two position-sensitive detectors give both energy- and angle-resolved photodouble ionization events. The size of the angular intervals into which the data is processed is chosen later to correspond with the available statistics. In this case 10° intervals in angle θ_i were used for all the presented data.

A significant development in this work has been the detection of electrons with unequal energies ($E_1 \neq E_2$) using a partially polarized photon beam obtained from a bending magnet. As demonstrated in the preceding section, measured TDCSs for those conditions are sensitive to the circularly polarized component of the incident radiation, which is notoriously difficult to measure in the far ultraviolet. Helium TDCS experiments to date, with $E_1 \neq E_2$, have therefore been usually performed on undulator beam lines where either S_1 (Schwarzkopf *et al* 1994, Bräuning *et al* 1998, Dörner *et al* 1998) or S_3 (Mergel *et al* 1998, Soejima *et al* 1999, Kheifets *et al* 1999) are very close to unity, or by placing the electron detectors in the same plane as the photon beam (Lablanquie *et al* 1995). Synchrotron radiation from a bending magnet has both left and right circular polarization contributions arising from light that comes from above and below the plane of the charged particles in the storage ring. Only the contribution that is emitted in the plane of the storage ring (nominally horizontal) will be 100% linearly polarized (i.e. $S_1 = 1$) and so $S_3 = 0$. (For a general discussion on synchrotron polarization properties see, for example, Schmidt (1997).) One could attempt to severely restrict the vertical acceptance angle from the synchrotron source to remove/minimize the S_3 component, but this will generally reduce the photon flux to a value which is unacceptably small for these coincidence experiments. An alternative approach, pursued in this work, is to ensure that the contributions from above and below the storage ring cancel out so giving a net S_3 of zero.

A recent modification to the beam line 3.3 allowed a moveable, narrow slit—of fixed width—to be inserted in between the monochromator input slit (optical 'window') and the grating. The slit was moved vertically through the light beam thus scanning the angle of divergence of the incoming radiation and S_1 was determined as a function of the slit position. This was done by measuring at $h\nu = 119$ eV the yield of photoelectrons associated with the $He^+(N = 1)$ state, whose β value is equal to 2 for all energies. The angle at which the yield was maximal (5° off horizontal) identifies the main axis of the polarization ellipse and the location of the first 10° wide sector whose yield was monitored separately. The other selected sector was displaced by 90° from the first. The efficiencies of the two sectors have been inter-calibrated by rotating the whole spectrometer through 45°. The results of these measurements are shown in figure 2(*a*). It should also be emphasized that these measurements were made after the light had traversed the grating and a ∼60 cm length of Pyrex capillary,

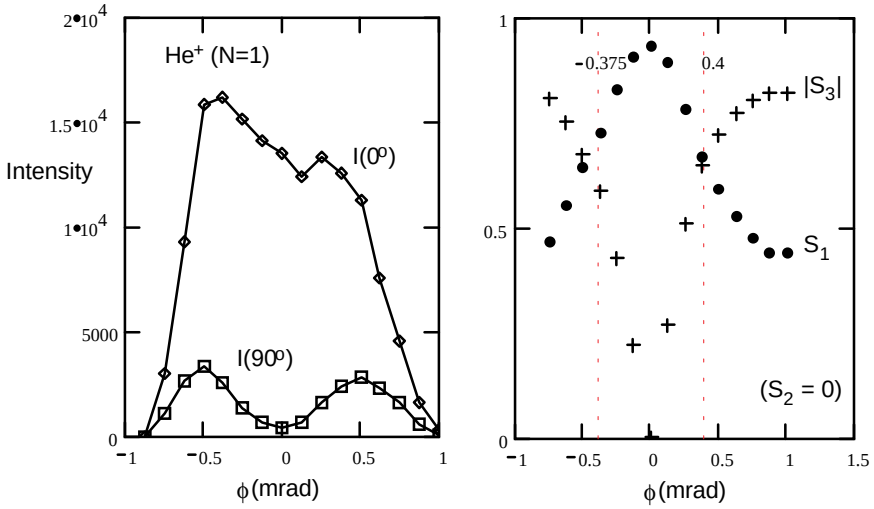

Figure 2. (*a*) The intensity of the $He^+(N = 1)$ line as a function of the divergence (ϕ) of the incoming radiation (with respect to the plane of the storage ring), measured by detecting the photoelectrons at $0 \pm 5^\circ$ and $90 \pm 5^\circ$ with respect to the major axis of the polarization ellipse. (*b*) A plot of the S_1 and $|S_3|$ values as obtained from the data in (*a*) (see the text). The vertical markers indicate the opening in the angular mask that was used when measuring the TDCSs, which balanced out the left and right circular polarization contributions.

and so correspond to the polarization properties at the interaction region. This is important as the light polarization can be changed by all the reflections it encounters on its way from the storage ring, which are also responsible for the measured tilt in the polarization ellipse.

As S_1, which is defined as $(I_{0^\circ} - I_{90^\circ})/(I_{0^\circ} + I_{90^\circ})$ (a procedure only valid for transitions with angular asymmetry parameter $\beta = 2$), is determined with respect to the tilted major axis of the polarization ellipse, S_2 is consequently zero. (This quantity is referred to as $\tilde{S}_1$ by Schmidt (1997).) The polarization state P, defined as $P = \sqrt{S_1^2 + S_2^2 + S_3^2}$, is not necessarily unity at the interaction region due to instrumental depolarization mentioned above. The value of P can be found by making the reasonable assumption that $S_3 = 0$ at the position of the maximum of the remarkably symmetric distribution of S_1, which essentially corresponds to light from the plane of the storage ring. Hence $|S_3|$ can be determined if this value of $P(= 0.94)$ is constant for all slit positions, as is done in figure 2(*b*). Alternatively, if the depolarization mechanism is strongest in the centre and gradually reduces on either side, $|S_3|$ can still be found by assuming an arbitrary, but symmetric, depolarization function. These two methods of determining $|S_3|$ can be regarded as a way of finding the overall uncertainly of our $|S_3|$ values. To ensure that the *net* circular polarization contribution to the measured TDCS should be zero, the $|S_3|$ values from figure 2(*b*) were multiplied by the corresponding intensities $(I_{0^\circ} + I_{90^\circ})$ and the grating was illuminated by balancing the accumulated yields of circularly polarized photons on each side of the minimum (which correspond to different helicity) to within 2%. Using this method our determination of the S_1 average was 0.82, and the net circular polarization contribution was estimated to yield $S_3 = 0 \pm 0.04$. Our experience is that the stability of the synchrotron over the duration of the TDCS measurements is remarkably good, therefore taking S_1 as 0.8 and S_3 as effectively 0 is justified.

The transmission function of the toroidal analysers as a function of the azimuthal angle θ was monitored after each change of electron energy (E_i) or focusing condition by observing the

image of the photoelectrons associated with the $He^+(N = 2)$ state for the same spectrometer tuning. The use of this satellite line whose β value varies with energy was preferred to the use of the He^+ main line ($N = 1$), since for the latter choice one would need to change the monochromator's grating between the calibration runs and the coincidence measurements. For the electron energies of 5, 10, 20, 30 and 35 eV we have used $\beta = 0.3, 0.57, 0.95, 1.2$ and 1.27, respectively. These values rely on the measurements by Wehlitz *et al* (1993) for electron energies above 15 eV and the near-threshold measurements by Hall *et al* (1991), to which a simple analytic form could be fitted. Estimated errors involved in this procedure are within $\Delta\beta = \pm 0.05$, which makes their effect comparable or smaller than the statistical error of the measured TDCS points. Another possible source of errors in the coincidence measurements, that could not be corrected by the above procedure, concerns the constancy of the interaction volume defined by the intersection of the photon beam, gas beam and the angular fields of view of the two toroidal analysers. This 'coincidence volume' was checked at the beginning of the run for the 'standard' 10 + 10 eV helium TDCS which can be accurately parametrized by a single correlation amplitude of the Gaussian form and the half-width of 91° (Schwarzkopf and Schmidt 1995, Malegat *et al* 1997b, Wightman *et al* 1998). After assuring that the coincidence volume was angle independent, only minor corrections to the input lens voltages were made between the consecutive adjustments of the electron optics for different electron energies.

Other experimental parameters that are relevant for the present study include the energy resolution and the subtraction of random coincidences. The energy resolution is characterized by the resolution of each electron analyser, which was 0.55 eV for the pass energy of 50 eV, and the photon beam resolution, which was ∼0.7 eV at the beam energy of 119 eV. In this experiment the average true coincidence rate, integrated over the full angular ranges of the electron analysers, was about 0.5 Hz, which was less than half the value we typically obtain at 20 eV. The time spectra featured the true coincidence peak of 40 ns FWHM and the randoms whose contribution over the 150 ns interval encompassing the true peak amounted to only 2–5%, the variations reflecting a strong dependence of the background counts on energy.

3. Theoretical

3.1. The 3C method

The 3C method is based on an ansatz for the final three-body continuum wavefunction in which the three pairs of Coulomb-interacting particles are treated in exactly the same way resulting essentially in a product of three Coulomb wavefunctions (see Maulbetsch and Briggs (1994) and references therein). A number of analytical properties of this wavefunction can be established. We briefly summarize the most important ones in the following:

- It shows the correct asymptotic behaviour, i.e. at all the particle separations r_1, r_2 and $R = |r_2 - r_1| \to \infty$ the 3C wavefunction converges to the correct asymptotic wavefunction given by Rosenberg (1973). From a theoretical point of view this is a very desirable property. However, it is not necessarily very relevant in PDI since the asymptotic region is not probed.
- The Kato cusp conditions are satisfied (Kato 1957). Due to the singularity of the Coulomb interaction, wavefunctions show a cusp as particle separation becomes very small. As any one of the three coordinates r_1, r_2 or $R \to 0$ while the other two remain finite the 3C wavefunction satisfies the Kato cusp conditions.
- The correct limiting wavefunctions are generated if some part of the interaction is 'switched off': if the electron–electron interaction is 'switched off' (the corresponding Sommerfeld

parameter is set to zero) the correct limit is obtained, and if the two electron–nucleus interactions are 'switched off' the correct limit is also reached.

- As mentioned before, the three two-body interactions are treated in exactly the same way and in the above-described sense these two-body systems are treated correctly.

For the initial bound state wavefunction we used a so-called correlated open-shell wavefunction as described in Maulbetsch and Briggs (1994). The method has been successfully applied to PDI in a series of publications of Maulbetsch and Briggs for both equal and unequal energy sharing and for the whole range of excess energies starting from threshold up to the high-energy limit.

The gauge sensitivity of the present results depends on both the θ_1 angle and the energy-sharing ratio. A special case is the $\theta_1 = 90^\circ$ TDCS, where a scaling factor of 0.087 brings the length-gauge TDCS into almost full agreement with the velocity-gauge result for each R. We have used this 'internal' scaling factor throughout this work to compare the 3C TDCS with relative measurements, in addition to the R-dependent 'external' scaling factors resulting from the comparisons of the 3C (velocity) with the CCC calculations (see sections 3.2 and 4).

3.2. The CCC method

The CCC method relies, to a much greater extent, on intensive computation. For the final state it attempts to solve the Schrödinger equation for the system of interest by employing the close-coupling (CC) expansion of the total wavefunction. In the particular case of the He PDI, this system consists of a photoelectron scattering on the He^+ ion. The inelastic scattering, which results in ejection of the remaining bound electron into the continuum, is responsible for the He PDI. Using a highly correlated Hylleraas-type ground state the CCC photoionization calculations are essentially gauge independent. The method yields a correctly integrated PDI cross section on a broad photon energy range which satisfies the Wannier threshold law and approaches the asymptotic limit of infinite photon energy (Kheifets and Bray 1998b).

The principal limitation of the CCC method is in its inability to satisfy the boundary conditions for infinite separation of the electrons and the residual ion. Owing to the discretization of the continuum using square-integrable pseudostates, the CC boundary conditions are the same as those of discrete excitation. The 'continuum' electron is modelled by a distorted Coulomb wave and the 'discrete' electron is modelled by a pseudostate obtained upon diagonalizing the He^+ Hamiltonian in an orthogonal Laguerre basis of size N. The ionization processes are identified with excitation of the positive-energy pseudostates. However, at any given total energy E this approach displays an apparent double-counting problem as pseudostates of energy E_2 and $E - E_2$ may be excited, thereby calculating the same ionization process twice, even though the formalism is unitary. Numerical investigation led to the suggestion that the amplitudes for excitation of pseudostates of energy $E - E_2$ ($E_2 < E/2$) should converge to zero for infinite basis sizes (Bray 1997), yielding a step-function singly differential (with respect to the energy) cross section (SDCS). For finite bases the SDCS was shown to have unphysical oscillatory behaviour whenever the size of the step (at $E/2$) was substantial. Furthermore, Stelbovics (1999) has shown that the CC estimate of the ionization amplitudes was like a Fourier expansion of a step-function with convergence at $E/2$ to half the true amplitude. He showed that for finite bases an unambiguous estimate of the ionization amplitude could only be extracted at $E/2$, unless the step-function was numerically accurately satisfied. It is indeed ironic that the CC formalism, which treats the outgoing electrons highly asymmetrically, is guaranteed to yield convergent absolute results only for the equal-energy sharing kinematics.

The unphysical oscillations of the SDCS, which affect the magnitude of the TDCS, require some attention. The combination of the value of the convergent equal-energy-sharing SDCS and the CCC(N) estimate of the total integrated cross section (TICS) allows one to approximate the SDCS on the whole secondary energy range by an integral-preserving quadratic. The raw CCC(N) results may then be rescaled (usually by not far from unity) to match the estimated SDCS. Note that since convergence in the TICS and SDCS($E/2$) is obtained for sufficiently large, but computationally tractable N, the quadratic estimate of the SDCS is independent of N. The SDCS($E/2$) is obtained after a coherent combination of the corresponding calculated amplitudes (Stelbovics 1999), which leads to an SDCS approximately a factor of two greater than the incoherent combination used earlier (Bray 1999).

In the present calculation the convergence in the angular distributions was achieved by increasing the number of the pseudostates to $17-l$ where the partial wave expansion of the slow ejected electron was performed with l up to 4, making a total of 60 pseudostates. The SDCS at $E_1 = E_2 = 20$ eV was found to be 0.32 kb eV^{-1} as compared to 0.35 kb eV^{-1} due to Pont and Shakeshaft (1995a). The TICS was 7.9 kb (7.8 kb by Pont and Shakeshaft 1995a). These two values, SDCS at $E_1 = E_2$ and TICS, and the assumption that the actual functional SDCS shape is a quadratic with its minimum at $E_1 = E_2$, allowed one to approximate the SDCS on the whole energy range of E_1. Thus, at the present excess energy of 40 eV the SDCS is rather flat as was previously established by Pont and Shakeshaft (1995a). The CCC results for asymmetric sharing of the available energy were then rescaled accordingly by factors of 0.76 at $E_1 = 10$ eV and 1.35 at $E_1 = 5$ eV, to yield the absolute TDCS values reported in the next section.

4. Results and discussion

The present experimental results, which were obtained in a single run over a period of about a week, essentially consist of three sets of experiments—each for a different choice of the energy sharing $R = E_2/E_1$ at 119 eV, i.e. 40 eV above the He^{2+} threshold.

4.1. TDCS for $E_1 = E_2 = 20$ eV

The equal-energy-sharing TDCSs obtained simultaneously at one orientation of the spectrometer are presented in figure 3. The experimental data are normalized to the results of the CCC calculations for $\theta_1 = 90^\circ$. The polarization vector (ϵ) lies in the horizontal direction, and the middle sector of the angular range of the small toroidal analyser was at $\theta_m = 115^\circ$. Each data point consists of a sum of all true coincident events recorded between a 10° wide sector centred around the specified position on the small analyser's detector and a sector of equal width on the large analyser's detector at the displayed θ_2 angle. Apart from corrections to the angular efficiency of the individual analysers (for an example see Reddish *et al* 1997a) no other adjustment in either angular efficiency variation or in normalization constant has been made throughout the entire set. The error bars reflect the statistical accuracy only. The overall agreement between experiment and the CCC theory is clearly excellent, especially for the widths and positions of the lobes and the evolution of their amplitudes with the θ_1 angle. A similar level of agreement exists with the 3C calculations in both gauges, which could hardly be resolved from the CCC results if multiplied by an 'external' scaling factor of 0.39 (for a discussion of the 3C gauge sensitivity see section 3.1). The present measurements show a small coincident signal in the region of the node, almost independent of the θ_1 angle. Although not shown in figure 3, when the CCC results were convoluted with the appropriate detection solid angles the observed filling-in of the node was fully reproduced (for the similar analysis

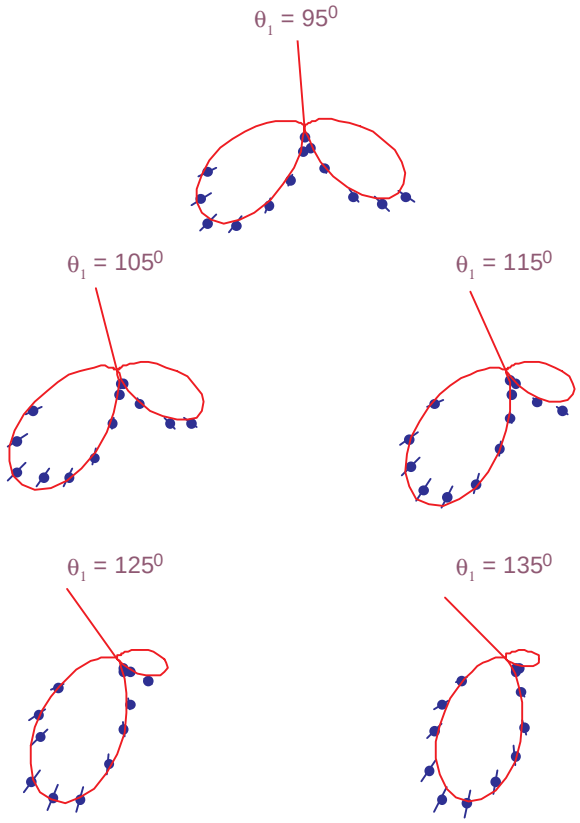

Figure 3. Five equal-energy TDCSs measured simultaneously and compared with the CCC calculation. The data are normalized to the theoretical TDCS for $\theta_1 = 95^\circ$. The cross section scale is indicated by the length of the line depicting the orientation of the first electron with respect to the polarization direction, which is equal to 6×10^{-24} cm^2 eV^{-1} sr^{-2}.

at $E = 20$ eV, see Reddish and Feagin (1999)).

In addition to the CCC and 3C calculations, we have also compared the data with the parametrization outlined in the introduction, by substituting

$$a_{\mathrm{u}}^{R=1} = 0, \qquad a_{\mathrm{g}}^{R=1} = \mathrm{e}^{-2\ln 2(\theta_{12}-\pi)^2/\theta_{1/2}^2} \tag{6}$$

for the transition amplitudes. The square of the a_{g} amplitude is a Gaussian with a half-width ($\theta_{1/2}$) of $103 \pm 2^\circ$, as found by fitting the whole data set shown in figure 3. Note that this value is higher than that obtained in our earlier preliminary studies (Reddish *et al* 1997b). The CCC and 3C TDCSs are practically indistinguishable from the parametrization, for all θ_1 angles, which provides further support for the Gaussian form for the correlation function. This may seem surprising considering that the Gaussian function emerged from an approximate, semiclassical treatment of the escaping electrons in a highly symmetrical Wannier configuration (Rau 1976, Kazansky and Ostrovsky 1993) which should prevail only very close to threshold.

4.2. $E_1 = 10$ eV, $E_2 = 30$ eV ($R = 3$)

Three sets of coincidence measurements have been made for this choice of unequal energy sharing, corresponding to the spectrometer orientations characterized by $\theta_{\mathrm{m}} = 110^\circ, 160^\circ$

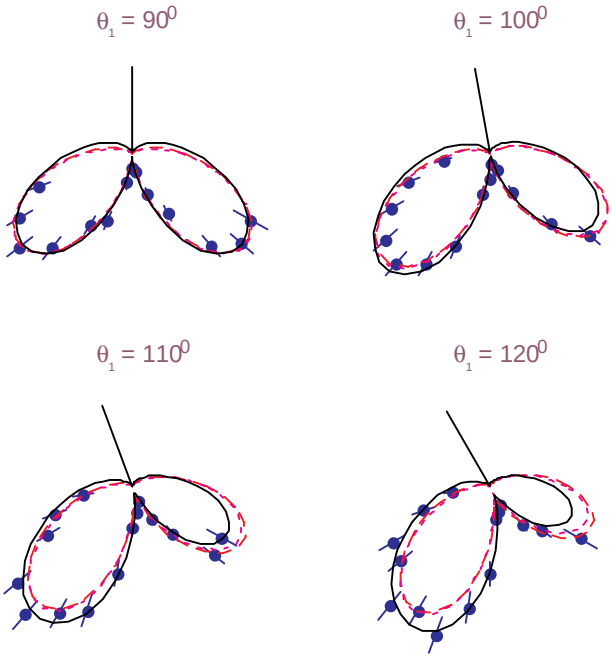

Figure 4. TDCSs in He at 40 eV for $E_1 = 10$ eV. All spectra correspond to the spectrometer orientation for which $\theta_m = 110^\circ$. The CCC calculations (full curve) provide the absolute scale, indicated by the length of the straight line showing the direction of the fixed angle electron ($= 6 \times 10^{-24}$ cm^2 eV^{-1} sr^{-2}). The experimental data and the 3C calculation in both gauges (velocity—dashed, length—dotted) are rescaled to the CCC result for $\theta_1 = 90^\circ$ (see the text).

and 200°. The spectra from the first orientation, which is very close to the one used for the equal energies (figure 3), are shown on figure 4. The theoretical and experimental TDCSs have been normalized to each other for the TDCS at $\theta_1 = 90^\circ$, as the agreement between the shapes of the calculated and measured TDCSs for that angle is excellent. We have chosen the cross section scale to be that of the CCC results, requiring an 'external' scaling factor for the 3C calculations of 0.41. The $\theta_1 = 90^\circ$ spectrum is virtually identical to the equivalent spectrum for the symmetric energy sharing. It is well known that for purely linearly polarized radiation (i.e. $S_1 = 1$) there is a node in the cross section irrespective of R if both electrons are emitted orthogonal to ε (Maulbetsch and Briggs (1995), see also equations (1) and (3) in the introduction). However, when $S_1 < 1$ a proportion of the $\theta_1 = 180^\circ$ TDCS is mixed in, which for $R \neq 1$ has no node at $\theta_{12} = \pi$. This results in a finite yield for the antiparallel emission, in addition to the filling of the node caused by the finite solid angles of the detectors. Although this filling-in is hardly discernible for $S_1 = 0.8$ and $R = 3$, it becomes more prominent as R increases (see figure 8). As the θ_1 angle departs from 90°, the size of the lobe (see figure 4) whose orientation approaches ε (i.e. the smaller lobe) diminishes rather less quickly than for the equal-energy case and the minimum between the two lobes becomes much shallower. Those same trends are very well represented by both theories, though a gradual departure between the individual results sets in as θ_1 approaches ε. Note that the gauge dependence of the 3C shapes for the conditions of figure 4 is very small.

Including the spectra from figure 4, altogether 18 individual TDCSs for that energy sharing were obtained spanning the whole range of θ_1 angles with enough overlap between

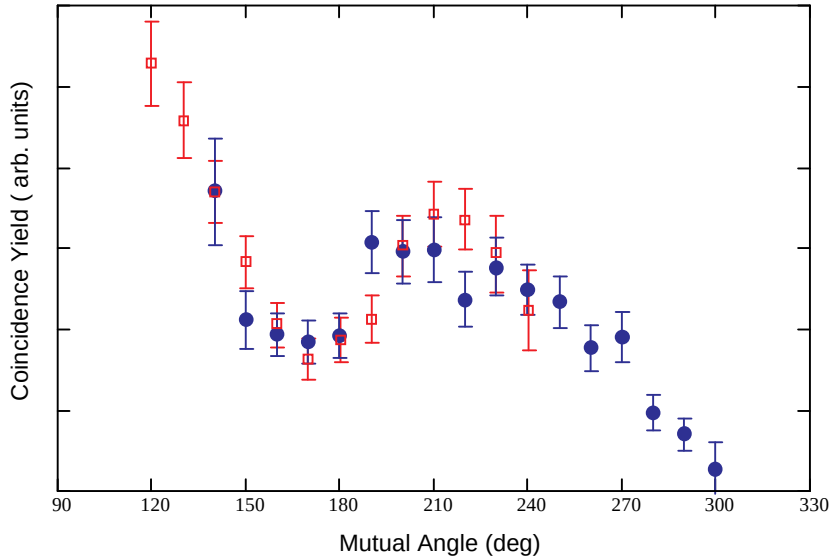

Figure 5. Combined spectrum consisting of the measured coincidence yields corresponding to $\theta_1 = 150^\circ$ (squares) and $\theta_1 = 210^\circ$ (circles), obtained at two different but physically equivalent orientations of the spectrometer (see the text).

the individual measurements to allow their inter-calibration. Observe also, that the other two orientations of the spectrometer ($\theta_m = 160^\circ$ and 200°) are physically equivalent, being symmetric with respect to ε, but that the corresponding θ_2 ranges differ (see figure 1). A joint analysis of the equivalent spectra from different spectrometer orientations enabled us to obtain the final TDCSs over larger θ_2 ranges than in the individual measurements and with better statistics in their central section where the constituent spectra overlap. An example is illustrated in figure 5, where the $\theta_1 = 150^\circ$ spectrum from the $\theta_m = 160^\circ$ set is compared with the equivalent orientation spectrum ($\theta_1 = 210^\circ$) from the $\theta_m = 200^\circ$ set after the inversion of the latter spectrum's angles around ε. The pleasing level of agreement where the spectra overlap provides supporting evidence for the constancy of the coincidence volume. It is also important to stress that we consider all spectra from the same orientation of the spectrometer to be automatically inter-calibrated, so that only one calibration constant is applied to each set. A similar level of agreement between the measured shapes and amplitudes is found for all 'equivalent' spectra, which are presented in figure 6, where the pairs of data points in the region of overlap have been replaced by their mean values.

The observed trends shown in figure 4 continue through the spectra presented in figure 6. In particular, the yield in the opposite direction to the slow electron grows in absolute terms until reaching its maximal value in the separate peak of the cross section for the $\theta_1 = 180^\circ$ TDCS. We will refer to the new maximum as the 'central lobe', to distinguish this feature of the TDCS from the two lobes of the equal-energy sharing case, which are separated by the node for the anti-parallel emission. Observe that for the θ_1 angles where these three lobes are clearly identifiable the position of the central lobe appears to hardly change with θ_1. Furthermore, quantitative comparison between the measurement and the calculations reveals differences in the overall intensity (i.e. *angle-integrated* cross section) and in the shape which increase as $\theta_1 \to \varepsilon$. Given the theories are normalized at $\theta_1 = 90^\circ$ they all predict a faster-than-measured reduction in the angle-integrated cross section as $\theta_1 \to \varepsilon$—the smallest and largest differences

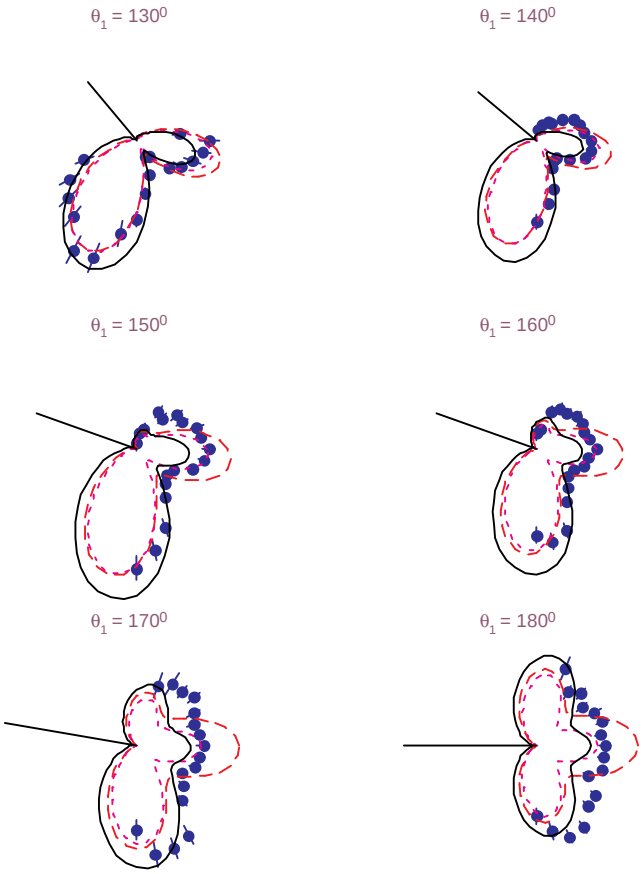

Figure 6. The second set of $R = 3$ TDCSs which contain the combinations between the measurements for different orientations of the spectrometer (see also figure 5). The experimental data and the 3C calculations in the velocity (dashed) and length (dotted) gauge have the same scaling with respect to the CCC theory (full curve) as in figure 4. The orientations of the 10 eV electron with respect to the polarization direction are shown by the straight lines, whose length corresponds to the cross section of 6×10^{-24} cm^2 eV^{-1} sr^{-2}.

corresponding to the velocity and the length gauge of the 3C theory, respectively. Another common feature of all theories is that they seem to predict a sharper depth to the minima between the central and the side lobes than is measured. In that respect the CCC and the 3C (velocity) are closer to the experiment than the 3C (length). In terms of the parametrization outlined in section 1, the depth of the minimum depends on the cosine of the phase difference ϕ between the a_u and a_g amplitudes, resulting in destructive interference for $90^\circ < \phi < 270^\circ$. The prominence of the central lobe, which is primarily related to the ratio between the ungerade and gerade amplitudes, varies most between the three calculations. The relative size of the central lobe is generally higher than measured, especially for the 3C (velocity gauge), while the CCC calculation seems to be closest to the measured sizes of the three lobes.

The presented comparison between the measurements and the theoretical calculations over the whole range of ejection angles for the slower electron at $R = 3$ shows the evolution of the characteristic three-pronged shape of the unequal-energy TDCS as a function of θ_1. For this choice of the final electron energies the effects of the energy asymmetry are still relatively

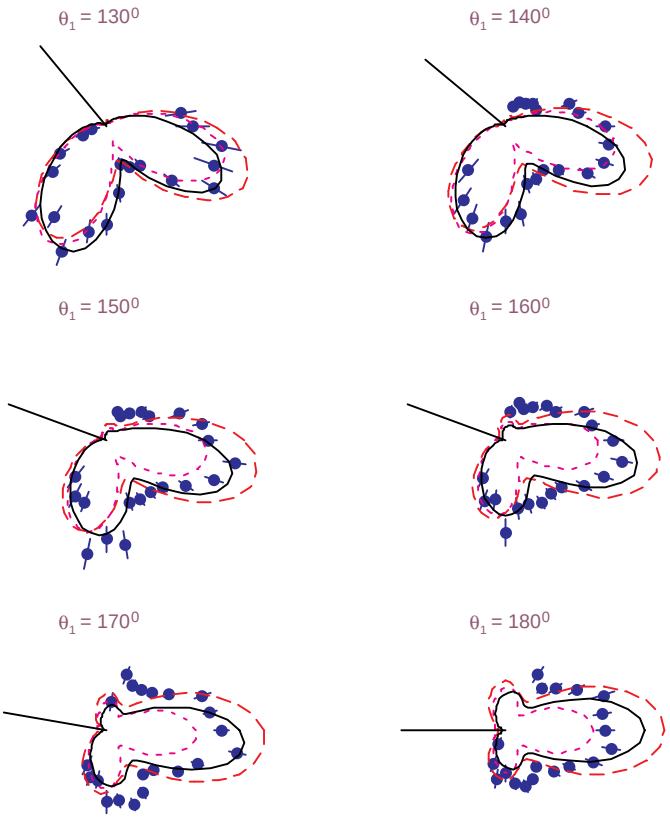

Figure 7. Angular distributions of the 35 eV electron for the indicated angles of the 5 eV electron. Measured points represent the combinations of two equivalent spectra measured at the spectrometer orientations of $\theta_m = 160^\circ$ and 200°. The data have been normalized to the absolute values of the CCC TDCS for $\theta_1 = 130^\circ$. The 3C curves (length—dotted, velocity—dashed) are rescaled to each other and to the CCC (full curve) at $\theta_1 = 90^\circ$ (see the text). The length of the bars indicating the angle of the slow electron corresponds to the cross section of 9×10^{-24} cm^2 eV^{-1} sr^{-2}.

small. The following section represents our measurements and calculations for the same total energy of 40 eV but for much larger differences between the energies of ejected electrons, thus focusing on the effects of the energy sharing.

4.3. $E_1 = 5$ eV, $E_2 = 35$ eV ($R = 7$)

For this ratio of ejected electron energies the measurements were conducted at the two symmetric orientations of the smaller toroid ($\theta_m = 160^\circ$ and 200°) which allow the angular range of θ_2 to be extended, as for the spectra for $R = 3$ shown in figure 6. A closer look at the six TDCSs shown in figure 7 reveals that the $R = 7$ data cover a somewhat larger angular range than the $R = 3$ measurements. This difference is due to the varying degree of success in compensating for the field-edge effects while tuning the detectors. The comparison with the calculations is made using the same methodology as for $R = 3$ (figures 4 and 6), namely the 3C TDCS in the length and velocity gauge have been normalized to the CCC $\theta_1 = 90^\circ$ result. The required 'external' scaling factor applied to the 3C TDCS is 0.58. However, at this energy-sharing ratio the differences in shape between the CCC and 3C TDCSs become

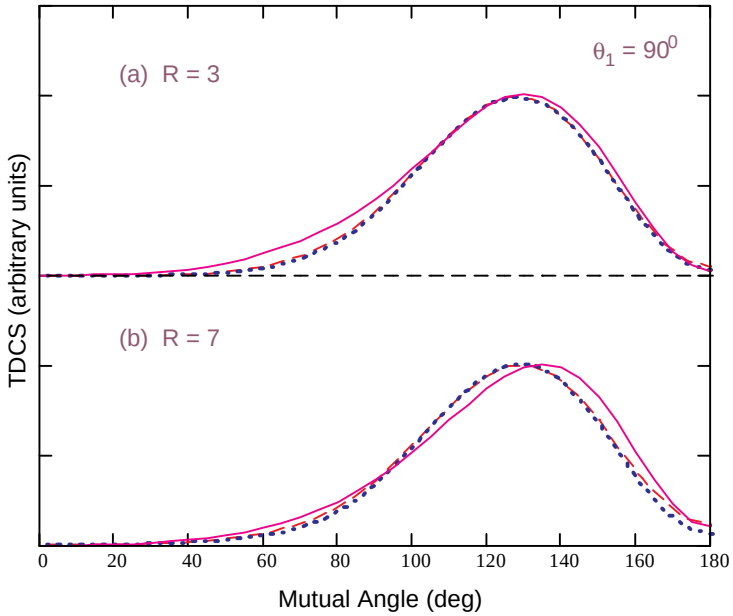

Figure 8. TDCS calculations (CCC—full line; 3C velocity—dashed; 3C length—dotted) at $\theta_1 = 90^\circ$ and $S_1 = 0.8$. (*a*) $E_1 = 5$ eV; (*b*) $E_1 = 10$ eV. The TDCSs are symmetric around $\theta_{12} = 180^\circ$. The 3C curves are separately normalized to the CCC at their maxima.

more noticeable, as shown in figure 8. Only half of the structure is shown, as the TDCS for $\theta_1 = 90^\circ$ has reflection symmetry about the $\theta_{12} = \pi$ direction. For $R = 3$, figure 8(*a*), only a minor difference in the region of small mutual angles can be noticed—the 3C cross section falling off faster than the CCC when θ_{12} is reduced. Note that an almost identical situation exists for $R = 1$, with the parametrized form (6) going in between the CCC and 3C results. For $R = 7$, figure 8(*b*), there is an additional change in the position of the CCC lobe maximum, while the 3C lobe remains virtually insensitive to R. At that particular geometry ($\theta_1 = 90^\circ$) the dynamical part of the TDCS (see equation (3)) can be factorized out as $|a_g + a_u|^2$. Consequently, any change of the TDCS shape with R implies a change in the θ_{12} dependence in one or both of the amplitudes from the Gaussian at $R = 1$. As our measurements for $R = 7$ did not cover that geometry, the question of experimental verification of this prediction of the CCC calculation remains open. The calculated $\theta_1 = 90^\circ$ TDCSs from figure 8 also show a relative increase of the yield for anti-parallel emission when R increases, due to incomplete polarization and the increased strength of the central lobe, as already mentioned in section 4.2. A noticeable difference between the 3C-length and -velocity forms at $\theta_{12} = \pi$ is due to the different ratio between the central and the side lobes in the two gauges, clearly shown in the last spectrum of figure 7.

Lacking the $\theta_1 = 90^\circ$ measurement, we have normalized our spectra in figure 7 to the lowest θ_1 TDCS available—that of $\theta_1 = 130^\circ$, where the differences between the calculations were smallest. Again, good agreement with respect to the main features of the calculated and measured TDCSs exists. At $\theta_1 = 130^\circ$ the lobe which was smaller for $R = 1, 3$ is now roughly equal to the other lobe. This observation is in excellent agreement with the CCC and the 3C (length) result. As with $R = 3$, the central lobe evolves as $\theta_1 \to \pi$, but is much more pronounced here than in the $R = 3$ case. The relative differences between calculations increase

too. As in the $R = 3$ case, when $\theta_1 \to \pi$ the overall (integrated) yield reduces much faster for the 3C (length) than for the velocity gauge calculations of the same theory. The measured intensity of the central lobe is best matched by the CCC theory, except in the $\theta_1 = 180^\circ$ case where the measured central lobe has a peculiar flat top. There is still a significant disagreement between the measurements and all the theories in the region where the central lobe meets the side lobes. This is especially apparent in TDCSs for $\theta_1 \geqslant 150^\circ$, where much deeper minima are predicted than measured. Another noticeable feature, which may be related to this, concerns the relative size of the side lobes in the calculated $\theta_1 = 170^\circ, 180^\circ$ TDCSs which are smaller than measured. We could demonstrate that the agreement between the CCC theory and the experiment in that respect improves significantly if smaller polarization is assumed, but the required S_1 value of $\sim$0.6 is well outside the anticipated error margin in the measurement (see figure 2 and the accompanying discussion).

4.4. Comparison with other work

Due to different kinematical conditions, the present asymmetric energy sharing results cannot be directly compared with the other work, but at least a qualitative discussion of the common features found in other related investigations is possible. The first reported measurements were conducted exclusively in a geometry where one of the electrons was collinear with the polarization direction, or very close to it. Of those, Dawber *et al* (1995) measured in the near-threshold region ($E \leqslant 2$ eV, $R \leqslant 12$), where the spectra were essentially equivalent despite the range of R. This confirms the expectation from the Wannier theory that $a_u \ll a_g$, when $E \to 0$. Schwarzkopf *et al* (1994) measured at relatively high photon energy ($E = 53$ eV) and for high electron energy ratio ($R \sim 10$). Under these conditions the central lobe, due to ungerade amplitude, dominates the cross section. All the theories (Maulbetsch and Briggs 1994, Pont and Shakeshaft 1995b, Kheifets and Bray 1998a) for that case showed good agreement with the relative data. In contrast, the measurements of Lablanquie *et al* (1995) at $E = 18.6$ eV and $R \sim 5$ are in the same class as the unequal-energy-sharing data reported here, i.e. featuring a balanced contribution from the a_g and a_u amplitudes. For those conditions the spectrum becomes sensitive not only to the ratio between the amplitudes but also to their phase difference, so presenting the greatest challenge. The data of Lablanquie *et al* (1995) (note that the subsequent measurements under similar conditions and with improved statistics have been reported by Mazeau *et al* 1996) have already been shown to disagree with most of the calculations (Pont *et al* 1996). The present measurements and their analysis are consistent with some of the aspects of Lablanquie *et al's* measurements, namely that the 3C theory predicts a relatively larger contribution to the central lobe then is measured, and that both 3C and 2SC calculations overestimate the minima between the central and the side lobes when the distribution of the faster electron is measured.

Recently, the absolute measurements of TDCSs in helium using the novel COLTRIMS technique have been reported (Dörner *et al* 1998, Bräuning *et al* 1998) for energies of 1, 6 and 20 eV above threshold and covering almost the entire phase space. They showed that the effects of the electron repulsion cause the three-dimensional TDCSs to peak for a coplanar geometry, with the measured shapes being almost insensitive to the out-of plane angle. Both the dynamical and the geometrical aspects of the three-dimensional TDCSs measured by Dörner *et al* 1998 have been rather successfully supported by the fourth-order Wannier theory of Feagin (1995,1996), especially at the two lower energies. That theory is capable of deriving the transition amplitudes directly (requiring only one empirical parameter for each total energy), which is an important feature from the aspect of parametrization as argued in the introduction. Note that the published spectra of Bräuning *et al* (1998) for $E = 20$ eV include the energy

partitioning case $R \sim 6$ which is similar to the measurements of Lablanquie *et al* (1995) at $E = 18.6$ eV and $R \sim 5$. The two results appear consistent, but the accuracy of the measurement may not be high enough judging by the internal inconsistency with the related TDCSs for the exchanged energies of the two electrons, as highlighted by comparison with the CCC theory. A similar combination of electron energies was also investigated by Mergel *et al* (1998) using the COLTRIMS technique with circular polarization of the light source. However, this latest result at $E = 20$ eV appears inconsistent (Berakdar 1999, Kheifets and Bray 1998c) with the measurements and CCC calculations for the equivalent linear polarization case of Bräuning *et al* (1998), mentioned above. Clearly, further measurements of higher accuracy are needed before the present controversy relating to these 20 eV results is resolved.

5. Conclusion

We have presented a detailed comparison between the 3C and CCC calculations and a comprehensive set of measured relative TDCSs in helium at $E = 40$ eV, providing the most rigorous test for theory to date. Internally normalized experimental data allowed a full study of θ_1 dependence within each investigated energy-sharing case ($R = 1, 3, 7$), enabling a systematic investigation of both the kinematics and the dynamics on the angular correlation patterns. For the strongest correlation case, that of the symmetric sharing of the available energy, all the theories are in perfect agreement with the data. This also includes the parametrization using a Gaussian correlation function of the half-width $\theta_{1/2} = 103 \pm 2^\circ$. This value confirms the trend measured earlier at much smaller energies—the correlation function width increases steadily with energy, but much slower than the Wannier $E^{1/4}$ power law predicted for the threshold region.

For asymmetric energy sharing ($R = 3, 7$) both theories show good overall agreement for the evolution of the TDCS shapes in the whole range of θ_1 and throughout the investigated range of electron dynamics, but a rather good statistical accuracy and overall consistency of the present experimental results brings into focus some quantitative differences. The 3C calculations in the two gauges (length and velocity) revealed differences between the relative shapes which increase with R, but only for θ_1 angles well away from 90°. It is interesting to note that the calculations in different gauges were often on different sides of the experiment, i.e. none could be clearly preferred. The calculations by the CCC are largely gauge independent and in this comparison generally occupy the middle ground, usually in better agreement with the experiment than the 3C. The remaining disagreements between the various theories and the experiment, highlighted by the present study, increase as θ_1 increases from about 140° to 180°. This is only partly due to our method of normalization, as it also concerns the ratio between the central and the side lobes and the depth of the minima between them. The latter feature is sensitive to the degree of linear polarization and will be better studied using the undulator radiation with $S_1 \cong 1$. The residual experimental uncertainties, concerning the polarization state, solid angle integration and the constancy of the coincidence volume, are not expected to alter these findings in any significant way.

Falling well short of attempting a full parametrization of the TDCS along the lines given in the introduction, it is still possible to paraphrase the above analysis in the language of parametrization: the present calculations seem to somewhat overestimate the ungerade amplitude relative to the gerade (especially the 3C-velocity gauge) and the inferred phase-difference angle ϕ is often too close to π (especially for the 3C-length gauge), causing too much destructive interference in the regions between the central and the side lobes. So far only the shape of the correlation function (for the symmetric energy sharing case) had its intuitive justification via the Wannier-model description of the Coulomb forces between the escaping

particles. It is hoped that the present results will stimulate more theoretical work leading to even better description of the helium TDCS for unequal energy sharing. This, in turn, might lead to an identification of a dynamical input into the relevant transition amplitudes governing the PDI, thus furthering our understanding of the role of electron correlations in that more general case.

Acknowledgment

The experimental group at Newcastle gratefully acknowledges EPSRC for their continued support for this work. We would also like to thank the Leverhulme Trust for a Fellowship for SC and Newcastle University for a Ridley Fellowship for JPW.

References

Berakdar J 1999 *J. Phys. B: At. Mol. Opt. Phys.* **32** L27–33
Berakdar J and Klar H 1992 *Phys. Rev. Lett.* **69** 1175
Berakdar J, Klar H, Huetz A and Selles P 1993 *J. Phys. B: At. Mol. Opt. Phys.* **32** 1463–78
Bräuning H *et al* 1998 *J. Phys. B: At. Mol. Opt. Phys.* **31** 5149–60
Bray I 1997 *Phys. Rev. Lett.* **78** 4721–4
——1999 *J. Phys. B: At. Mol. Opt. Phys.* submitted
Brion C E and Thomas G E 1968 *Phys. Rev. Lett.* **20** 241–2
Cvejanović S and Read F H 1974 *J. Phys. B: At. Mol. Phys.* **7** 1841–52
Dawber G, Avaldi L, McConkey A G, Rojas H, MacDonald M A and King G C 1995 *J. Phys. B: At. Mol. Opt. Phys.* **28** L271–7
Dörner R *et al* 1998 *Phys. Rev.* A **57** 1074–90
Feagin J M 1995 *J. Phys. B: At. Mol. Opt. Phys.* **28** 1491–516
——1996 *J. Phys. B: At. Mol. Opt. Phys.* **29** L551–8
Hall R I, Avaldi L, Dawber G, Zubek M, Ellis K and King G C 1991 *J. Phys. B: At. Mol. Opt. Phys.* **24** 115–25
Huetz A, Lablanquie P, Andrić L, Selles P and Mazeau J 1994 *J. Phys. B: At. Mol. Opt. Phys.* **27** L13–8
Huetz A, Selles P, Waymel D and Mazeau J 1991 *J. Phys. B: At. Mol. Opt. Phys.* **24** 1917–33
Kato T 1957 *Commun. Pure Appl. Math.* **10** 151
Kazansky A K and Ostrovsky V N 1993 *J. Phys. B: At. Mol. Opt. Phys.* **26** 2231–44
——1994 *J. Phys. B: At. Mol. Opt. Phys.* **27** 447–60
——1995a *Phys. Rev.* A **51** 3698–702
——1995b *J. Phys. B: At. Mol. Opt. Phys.* **28** 1453–62
Kheifets A S and Bray I 1998a *J. Phys. B: At. Mol. Opt. Phys.* **31** L447–53
——1998b *Phys. Rev.* A **58** 4501–11
——1998c *Phys. Rev. Lett.* **81** 4588–91
Kheifets A S, Bray I, Soejima K, Danjo A, Okuno K and Yagishita A 1999 *J. Phys. B: At. Mol. Opt. Phys.* **32** l501–9
Krässig B, Schwarzkopf O and Schmidt V 1993 *J. Phys. B: At. Mol. Opt. Phys.* **26** 2589–99
Lablanquie P, Mazeau J, Andric L, Selles P and Huetz A 1995 *Phys. Rev. Lett.* **74** 2192–5
Lucey S P, Rasch J, Whelan C T and Walters H R J 1998 *J. Phys. B: At. Mol. Opt. Phys.* **31** 1237–58
Malegat L, Selles P and Huetz A 1997a *J. Phys. B: At. Mol. Opt. Phys.* **30** 251–61
Malegat L, Selles P, Lablanquie P, Mazeau J and Huetz A 1997b *J. Phys. B: At. Mol. Opt. Phys.* **30** 263–76
Maulbetsch F and Briggs J S 1993 *J. Phys. B: At. Mol. Opt. Phys.* **26** 1679–96
——1994 *J. Phys. B: At. Mol. Opt. Phys.* **27** 4095–104
——1995 *J. Phys. B: At. Mol. Opt. Phys.* **28** 551–64
Maulbetsch F, Pont M, Briggs J S and Shakeshaft R 1995 *J. Phys. B: At. Mol. Opt. Phys.* **28** L341–7
Mazeau J, Andric L, Jean A, Lablanquie P, Selles P and Huetz A 1996 *Atomic and Molecular Photoionization* ed A Yagishita and T Sasaki (Tokyo: Universal Academy) pp 31–8
Mazeau J, Lablanquie P, Selles P, Malegat L and Huetz A 1997 *J. Phys. B: At. Mol. Opt. Phys.* **30** L293–9
Mergel V *et al* 1998 *Phys. Rev. Lett.* **70** 5301–4
Peterkop R 1971 *J. Phys. B: At. Mol. Phys.* **4** 513–21
Pont M and Shakeshaft R 1995a *J. Phys. B: At. Mol. Opt. Phys.* **28** L571–7
——1995b *Phys. Rev.* A **51** R2676–9

Pont M, Shakeshaft R, Maulbetsch F and Briggs J S 1996 *Phys. Rev.* A **53** 3671–4
Rau A R P 1971 *Phys. Rev.* A **4** 207–20
——1976 *J. Phys. B: At. Mol. Phys.* **9** L283–8
Reddish T J and Feagin J M 1999 *J. Phys. B: At. Mol. Opt. Phys.* **32** 2473–86
Reddish T J, Richmond G, Bagley G W, Wightman J P and Cvejanović S 1997a *Rev. Sci. Instrum.* **68** 2685–92
Reddish T J, Wightman J P and Cvejanović S 1997b *Physics of Ionized Gases* ed B Vujičič, S Djurović and J Purić (Novi Sad: Institute of Physics) pp 114–52
Rosenberg L 1973 *Phys. Rev.* D **8** 1833
Schaphorst S J, Krässig B, Schwarzkopf O, Sherer N, Schmidt V, Lablanquie P, Andric L, Mazeau J and Huetz A 1995 *J. Electron Spectrosc.* **76** 229–35
Schmidt V 1997 *Electron Spectrometry of Atoms using Synchrotron Radiation* (Cambridge: Cambridge University Press)
Schmidt V 1998 *Photonic Electronic and Atomic Collisions* ed F Aumayr and H Winter (Singapore: World Scientific) pp 85–96
Schwarzkopf O, Krässig B, Elmiger J and Schmidt V 1993 *Phys. Rev. Lett.* **70** 3008–11
Schwarzkopf O, Krässig B, Schmidt V, Maulbetsch F and Briggs J S 1994 *J. Phys. B: At. Mol. Opt. Phys.* **27** L347–50
Schwarzkopf O and Schmidt V 1995 *J. Phys. B: At. Mol. Opt. Phys.* **28** 2847–62
Soejima K, Danjo A, Okuno K and Yagishita A 1999 *Phys. Rev. Lett.* **83** 1546–9
Stelbovics A T 1999 *Phys. Rev. Lett.* **83** 1570–3
Viefhaus J, Avaldi L, Heiser F, Hentges R, Gessner O, Rüdel A, Wiedenhöft M, Wieliczek K and Becker U 1996a *J. Phys. B: At. Mol. Opt. Phys.* 29 L729
Viefhaus J *et al* 1996b *Phys. Rev. Lett.* **77** 3975
Vinkalns I and Gailitis M 1967 *Proc. 5th Int. Conf. on Physics of Electronic and Atomic Collisions* (Leningrad: Nauka) pp 648–50
Wannier G H 1953 *Phys. Rev.* **90** 817–25
Wehlitz R, Langer B, Berrah N, Whithfield S B, Viefhaus J and Becker U 1993 *J. Phys. B: At. Mol. Opt. Phys.* **26** L783–8
Wightman J P, Cvejanović S and Reddish T J 1998 *J. Phys. B: At. Mol. Opt. Phys.* **31** 1753–64